

Gamow–Teller strength in ^{56}Fe nucleus at finite temperatures

Esra YÜKSEL^{1,2,*}

¹Department of Physics, Faculty of Science, University of Zagreb, Zagreb, Croatia

²Department of Physics, Faculty of Science, Yıldız Technical University, Esenler, İstanbul, Turkey

Received: 18.04.2018

Accepted/Published Online: 13.09.2018

Final Version: 12.10.2018

Abstract: In this work, the effect of temperature on Gamow–Teller strength is investigated using fully self-consistent finite temperature proton-neutron random phase approximation in the ^{56}Fe nucleus. The calculations are performed with Skyrme-type SkM* interaction at $T = 0, 1$, and 2 MeV. It is shown that temperature effects of the occupation probabilities of states and new excitation channels become possible due to the smearing of the Fermi surface. The Gamow–Teller excitation energies shift downward and new excited states are also obtained in the low-energy region due to the unblocked transitions at high temperatures.

Key words: Hartree–Fock, random phase approximation, finite temperatures, Gamow–Teller excitations

1. Introduction

Spin-isospin excitations in nuclei are known as one of the most important excitation modes in nuclei, not only for nuclear physics but also for nuclear astrophysics [1–3]. Among the spin-isospin excitations, the Gamow–Teller (GT) resonances ($\Delta L = 0, J^\pi = 1^+$) are the most widely known, both experimentally [4,5] and theoretically [6–14]. Apart from their importance to understand the structure of nuclei and nuclear interaction, it is also known that the GT resonances play a dominant role in the calculation of nuclear weak interactions processes like beta decay, electron capture, and charged-current neutrino-nucleus reactions [15–19]. For instance, the electron capture rates are sensitive to the excitation energy and the strength of the GT $^+$ resonance of nuclei with mass $A \approx 60$. Therefore, accurate determination of the nuclear properties and the GT excitations is quite important for astrophysical calculations. In addition, it is known that nuclear weak interaction processes occur at finite temperatures from several hundreds of keV to MeV. Therefore, the temperature effects should also be included in the calculations.

Proton-neutron random phase approximation (PNRPA) is known as an efficient and reliable tool in the description of the collective excitations in nuclei (e.g., GT transitions) [6–12]. Recently, the effect of temperature on GT $^+$ strength and electron capture was investigated at zero and finite temperatures using the relativistic [20] and nonrelativistic [21,22] functionals. In addition, evolution of the GT $^+$ distributions with increasing temperature was studied using PNRPA extended to finite temperature by the thermo-field-dynamics formalism [23]. In this work, I aim to investigate the effect of temperature on both the ground state properties and Gamow–Teller GT $^+$ and GT $^-$ strength distributions in the ^{56}Fe nucleus using fully self-consistent finite temperature PNRPA. This nucleus is known to be important in the calculation of the electron capture cross-sections and rates that take place in stellar environments.

*Correspondence: eyuksel@yildiz.edu.tr

The paper is organized as follows. In Section 2, finite temperature PNRPA is briefly summarized and the details of the calculations are provided. In Section 3, the results are presented for the GT strength distributions both at zero and finite temperatures. The changes in the strength and the excitation energies are analyzed and the physical mechanism behind these changes is discussed in detail. Finally, a summary and conclusions are given in Section 4.

2. Microscopic model: finite temperature PNRPA

In the present work, ground state properties are calculated using the finite temperature Hartree–Fock approach (FT-HF) and Skyrme-type SkM* [24] interaction. The SkM* interaction is known to be successful in the description of the GT strength in nuclei [25]. In the FT-HF method, the occupation probabilities of the states obey the temperature-dependent Fermi–Dirac distribution function at finite temperatures [26]:

$$f_i = [1 + \exp(\varepsilon_i - \lambda/k_B T)]^{-1}, \quad (1)$$

where ε_i is the single-particle energies of the states and λ is the chemical potential for proton or neutrons. In addition, k_B and T represent the Boltzman constant and temperature, respectively. In order to study the spin-isospin excitations in nuclei at finite temperatures, the PNRPA should be extended to finite temperature PNRPA. At finite temperatures, the PNRPA matrix reads as follows [20]:

$$\begin{pmatrix} A_{pnp'n'}^J & B_{pnp'n'}^J \\ -B_{pnp'n'}^J & -A_{pnp'n'}^J \end{pmatrix} \begin{pmatrix} X_{p'n'}^J \\ Y_{p'n'}^J \end{pmatrix} = E_\nu \begin{pmatrix} X_{pn}^J \\ Y_{pn}^J \end{pmatrix}, \quad (2)$$

where A and B are defined as

$$A_{pnp'n'}^J = (\varepsilon_P - \varepsilon_H) \delta_{pp'} \delta_{nn'} + (u_p v_n u_{p'} v_{n'} + v_p u_n v_{p'} u_{n'}) V_{pn'np'}^{ph} \sqrt{|f_n - f_{p'}|} \sqrt{|f_{n'} - f_{p'}|} \quad (3)$$

$$B_{pnp'n'}^J = (u_p v_n v_{p'} u_{n'} + v_p u_n u_{p'} v_{n'}) V_{pn'np'}^{ph} \sqrt{|f_n - f_{p'}|} \sqrt{|f_{n'} - f_{p'}|} \quad (4)$$

Here, P and H represent the particle and hole, respectively. The particle and hole can be either protons (p) or neutrons (n), depending on the type of excitation. In the matrices, $V_{pn'np'}^{ph}$ represents the residual particle-hole interaction, while the u and v factors are defined in order to separate the proton-neutron and neutron-proton excitations. These factors are defined as $u_p = 1$, $v_p = 0$, $u_n = 0$, $v_n = 1$ for the neutron-proton ($f_n > f_p$) excitations and $u_p = 0$, $v_p = 1$, $u_n = 1$, $v_n = 0$ for the proton-neutron ($f_n < f_p$) excitations. In this way, GT^- and GT^+ excitations are decoupled from each other. After the diagonalization of the FT-PNRPA matrices, one obtains the excitation energies (E_ν) with the corresponding forward-going (X_{pn}^J) and backward-going amplitudes (Y_{pn}^J). The strength functions for the GT^- and GT^+ cases are calculated using

$$B_\nu^{J(GT^-)} = \left| \sum_{pn} (X_{pn}^J u_p v_n + Y_{pn}^J v_p u_n) \langle p \parallel T^- \parallel n \rangle \sqrt{|f_{n'} - f_{p'}|} \right|^2 \quad (5)$$

$$B_\nu^{J(GT^+)} = \left| \sum_{pn} (X_{pn}^J v_p u_n + Y_{pn}^J u_p v_n) \langle n \parallel T^+ \parallel p \rangle \sqrt{|f_{n'} - f_{p'}|} \right|^2 \quad (6)$$

where the spin-isospin operator is $T^\mp = \sum_{i=1}^A \sigma_i \tau_i^\mp$ for the GT^\mp excitations. In the calculations, the Ikeda sum rule [13] is also satisfied at each temperature:

$$\sum B(GT^-) - \sum B(GT^+) = 3(N - Z). \quad (7)$$

The calculations are self-consistent; namely, the same interaction is used both in the ground state and in excited state calculations.

3. Results and discussion

In this section, the effect of the temperature on the GT excitations in the ^{56}Fe nucleus is analyzed and discussed. It is known that the pairing correlations in nuclei disappear after the critical temperatures [27–30]. In this work, the calculations are performed at high temperatures at $T = 1$ and 2 MeV. Therefore, the FT-HF and FT-PNRPA methods are appropriate in order to investigate the effect of the temperature on the GT strength. Before starting to discuss the effect of the temperature on the GT states in nuclei, it is also necessary to understand the changes in the ground state properties of the ^{56}Fe nucleus by increasing temperature.

In Figure 1, the occupation probabilities of neutron and proton states are displayed with respect to the single-particle energies of the selected states around the Fermi level for the ^{56}Fe nucleus. The calculations are performed using the FT-HF method at $T = 0, 1$, and 2 MeV, respectively. In order to avoid the unphysical neutron (proton) vapor problem, the calculations are performed up to $T = 2.0$ MeV [26]. At $T = 0$ MeV, occupation probabilities are zero for neutron (proton) $2p_{1/2}, 1f_{5/2}$, and $1g_{9/2}$ states ($2p_{3/2}, 2p_{1/2}, 1f_{5/2}$). By increasing temperature, the occupation probabilities of the states start to change around the Fermi level. While the occupation probabilities of states decrease below the Fermi level, the occupation probabilities of the states increase above the Fermi level with increasing temperature. This effect leads to the smearing of the Fermi surface and opens new excitation channels for the spin-isospin excitations. Therefore, apart from the particle-hole (ph) excitations, particle-particle (pp) and hole-hole (hh) excitations also start to play a role in the excitations at finite temperatures. While the pp excitations refer to the transitions above the Fermi level, hh excitations refer to the transitions below the Fermi level. The impact of the smearing of the Fermi surface on the GT excitations will also be discussed below. On the other hand, the single-particle energies are barely affected with increasing temperature. The effect of the temperature on the occupation probabilities and single-particle energies is stronger at higher temperatures, and especially after $T = 1.0$ MeV.

In Figure 2, the GT^- strength is displayed for the ^{56}Fe nucleus at $T = 0, 1$, and 2 MeV. At $T = 0$ MeV, the main GT^- peak is obtained at 17.22 MeV. Two direct spin-flip transitions, $\nu 1f_{7/2} \rightarrow \pi 1f_{5/2}$ (75.3%) and $\nu 2p_{3/2} \rightarrow \pi 4p_{1/2}$ (13.1%), and one core polarization transition, $\nu 2p_{3/2} \rightarrow \pi 4p_{3/2}$ (10.3%), are feeding this state. Here, π and ν refer to proton and neutron, respectively. In the low-energy region, two states are found with considerable strengths at 6.72 and 8.48 MeV. The peak at 6.72 MeV is formed with two core polarization transitions: $\nu 1f_{7/2} \rightarrow \pi 1f_{7/2}$ (63.1%) and $\nu 2p_{3/2} \rightarrow \pi 2p_{3/2}$ (35.1%). The state at 8.48 MeV is only formed with one direct spin-flip transition: $\nu 2p_{3/2} \rightarrow \pi 2p_{1/2}$ (97.9%) at zero temperature.

By increasing temperature, the first thing to notice is the shift in the main GT^- peak energy towards lower energies. This effect becomes more pronounced after $T = 1$ MeV. In addition, formation of the new excited states can be seen below the main GT^- peak. At $T = 2.0$ MeV, the GT^- peak is found at 16.65 MeV. Apart from the $\nu 1f_{7/2} \rightarrow \pi 1f_{5/2}$ (89.3%) and $\nu 2p_{3/2} \rightarrow \pi 4p_{1/2}$ (1.3%) transitions, this state also takes a

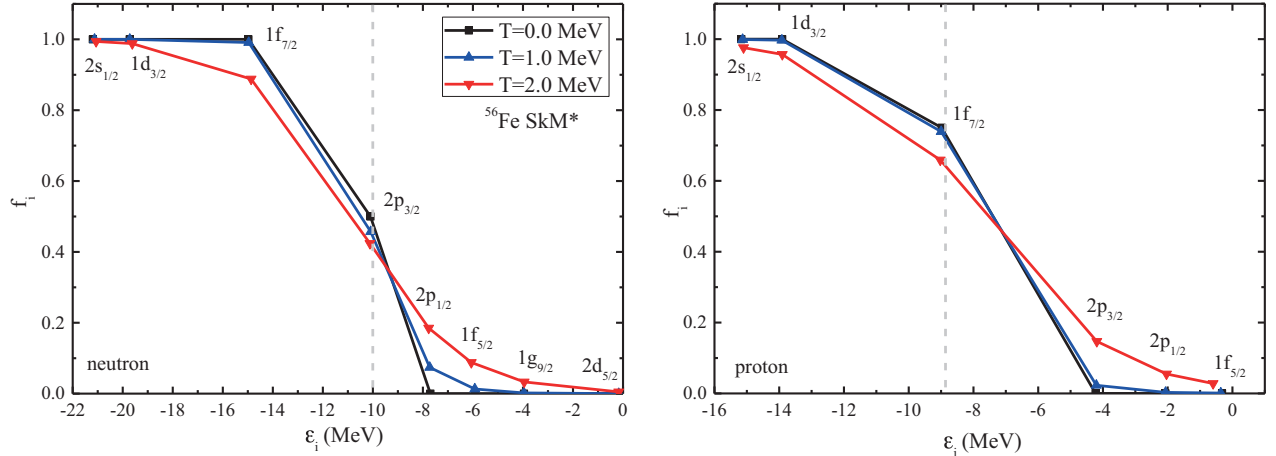


Figure 1. Upper panel: Occupation probabilities for neutrons as a function of temperature around the Fermi level. The calculations are performed using the finite temperature Hartree–Fock method at $T = 0, 1$, and 2 MeV for the ^{56}Fe nucleus. Lower panel: Same but for protons. The gray dashed lines indicate the Fermi level for neutrons and protons at zero temperature.

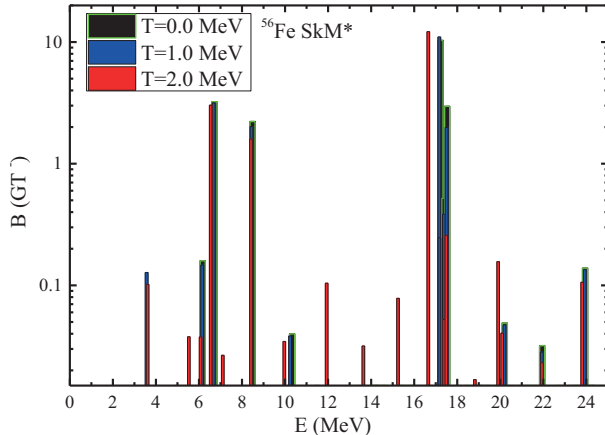


Figure 2. The GT⁻ strength distributions for the ^{56}Fe nucleus with respect to the excitation energy of the parent nucleus. Calculations are performed with the finite temperature PNRPA using Skyrme-type SkM* interaction at $T = 0, 1$, and 2 MeV, respectively.

contribution from $\nu 1g_{9/2} \rightarrow \pi 3g_{7/2}$ (5.7%). The contribution of the latter is related to the changing occupation probabilities of the states ($\nu 1g_{9/2}$) and the opening of the new excitation channels at finite temperatures, as mentioned above. In addition, the change in the energy of the main GT⁻ strength peak is about 0.57 MeV from $T = 0$ to $T = 2.0$ MeV. Second, the temperature also affects the low-energy region of the GT⁻ strength. The excited state energies shift slightly downwards by increasing temperatures. After $T = 1.0$ MeV, formation of the new excited states can also be seen in the low-energy region (see Figure 2). Therefore, the strength in the low-energy region also increases slightly. These changes in the excitation energies and strength can affect the r-process nucleosynthesis.

The GT⁺ strength distribution is also displayed in Figure 3. At $T = 0$ MeV, the main peak is obtained at 4.95 MeV, which is only formed with direct spin-flip $\pi 1f_{7/2} \rightarrow \nu 1f_{5/2}$ single-particle transition. The results from the large-scale shell model (LSSM) calculations [16] and the experimental data [5] are also provided. The

FT-PNRPA results are in agreement with the LSSM results in terms of the location of the centroid energies. Since the calculations do not involve more complex configurations (like 2p-2h) than single-particle configurations, PNRPA is not able to produce the experimental data accurately. Therefore, the GT^+ state is obtained as a single strong peak. Nonetheless, the centroid energy of the GT^+ excitation is lying within the experimental data.

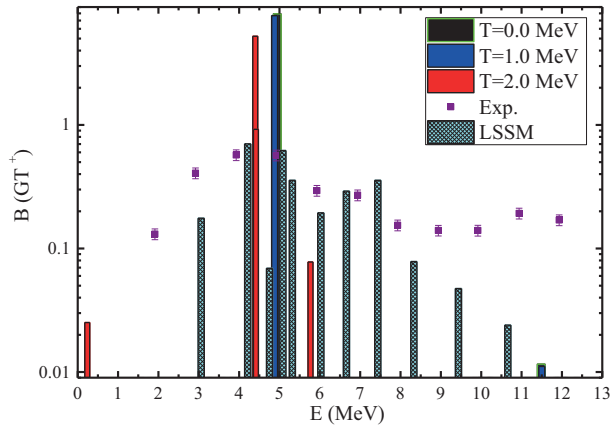


Figure 3. Same as in Figure 2, but for GT^+ strength.

By increasing the temperature, the main excited state excitation energy shifts downwards and formation of the new excited states can be seen from Figure 3. Although the impact of the temperature is not much in the low-energy strength, the decrease in the excitation energies and slight increase in strength is shown to be important for astrophysical processes, such as in the calculation of electron capture rates [19–23].

In order to gain a more physical insight about the effect of temperature on the low-energy region, the major low-energy excited states are analyzed at $T = 0, 1$, and 2 MeV. In Tables 1 and 2, the excitation energies, transitions, and their contribution for a given excited state are provided in percentage for GT^- and GT^+ excitations, respectively. The first thing to notice is the decrease in the excitation energies of the states with increasing temperature. In addition, the transitions for the major low-energy excited states almost do not change at $T = 0$ and 1 MeV. At $T = 2$ MeV, the GT^- excitation at $E = 6.55$ MeV starts to take a contribution from the $\nu 1g_{9/2} \rightarrow \pi 1g_{9/2}$ transition. Similarly, the GT^+ excitation at $E = 4.39$ MeV also starts to take a contribution from the $\pi 1f_{5/2} \rightarrow \nu 4p_{3/2}$ transition at $T = 2$ MeV. As explained above, the contribution of these transitions is related to the occupation of the states above the Fermi level (see Figure 1) and the opening of the new excitation channels with increasing temperature.

As mentioned above, the formation of the new low-energy excited states is also obtained at $T = 2$ MeV. In Table 3, these new low-energy excited states with considerable strengths are given. The transitions and their contributions for these excited states are also provided in percentages. Apparently, new low-energy states are mainly formed with one single-particle transition and do not display collectivity. In the low-energy region, most of the transitions have either pp or hh nature and occur due to the smearing of the Fermi surface by increasing temperature.

Table 1. The major low-energy states for GT^- excitations in the ^{56}Fe nucleus at $T = 0, 1$, and 2 MeV. The excited states, transitions, and their contribution ($X^2 - Y^2$) for a given excited state are also provided in percentages. Asterisk indicates the unblocked transitions that start to contribute at finite temperatures. Herein, π and ν represent proton and neutron, respectively.

Transitions for the excited states at	$T = 0.0$ MeV $E = 6.72$ MeV	$T = 1.0$ MeV $E = 6.68$ MeV	$T = 2.0$ MeV $E = 6.55$ MeV
$\nu 1f_{7/2} \rightarrow \pi 1f_{7/2}$	63.1	65.2	58.3
$\nu 2p_{3/2} \rightarrow \pi 2p_{3/2}$	35.1	31.9	29.6
$\nu 1g_{9/2} \rightarrow \pi 1g_{9/2}^*$	-	-	5.4
For the excited states at	$E = 8.48$ MeV	$E = 8.44$ MeV	$E = 8.42$ MeV
$\nu 2p_{3/2} \rightarrow \pi 2p_{3/2}$	97.9	98.2	98.6

Table 2. Same as in Table 1, but for GT^+ excitation.

Transitions	$T = 0.0$ MeV	$T = 1.0$ MeV	$T = 2.0$ MeV
for the excited states at	$E = 4.95$ MeV	$E = 4.88$ MeV	$E = 4.39$ MeV
$\pi 1f_{7/2} \rightarrow \nu 1f_{5/2}$	99.9	99.9	83.2
$\pi 1f_{5/2} \rightarrow \nu 4p_{3/2}^*$	-	-	14.8

Table 3. The selected low-energy states for GT^+ and GT^- excitations in the ^{56}Fe nucleus at $T = 2.0$ MeV. The transitions and their contributions for a given excited state are also provided in percentages. Asterisk indicates the unblocked transitions that start to contribute at finite temperatures.

	Low-energy states	Transitions	%
GT^+	$E = 0.24$ MeV	$\pi 1d_{5/2} \rightarrow \nu 1d_{3/2}^*$	99.8
	$E = 4.42$ MeV	$\pi 1f_{7/2} \rightarrow \nu 1f_{5/2}$ $\pi 1f_{5/2} \rightarrow \nu 4p_{3/2}^*$	14.5 85.1
GT^-	$E = 3.61$ MeV	$\nu 2p_{1/2} \rightarrow \pi 2p_{3/2}^*$	99.9
	$E = 5.52$ MeV	$\nu 1f_{5/2} \rightarrow \pi 1f_{5/2}^*$ $\nu 1d_{3/2} \rightarrow \pi 1d_{3/2}$	94.3 3.6
	$E = 11.93$ MeV	$\nu 1d_{5/2} \rightarrow \pi 1d_{3/2}^*$	98.9

4. Summary and conclusions

The effect of the temperature on the GT excitations in the ^{56}Fe nucleus was investigated using fully self-consistent finite temperature PNRPA. The Skyrme-type SkM* interaction was employed in the calculations, which was able to produce the experimental centroid energy for GT^+ excitation in the ^{56}Fe nucleus at zero temperature.

It was shown that the temperature lowers the energies of the excited states and increases strength in the low-energy region. The principal reason for these changes is the opening of the new excitation channels due to the smearing of the Fermi surface at finite temperatures. Therefore, unblocked transitions become possible at finite temperatures. In addition, the new excited states are found to be noncollective and mainly formed by pp and hh single-particle transitions above and below the Fermi level, respectively. While the effect of temperature is negligible below $T = 1$ MeV, its effect is more pronounced at higher temperatures.

Finite temperature PNRPA is known as an appropriate tool in the investigation of excitations of closed shell nuclei. For open shell nuclei, inclusion of the pairing correlations both in the ground state and excited states is necessary, which is omitted in this work in order to disentangle the effect of temperature clearly. In addition, these calculations should be performed at very low temperatures, at which pairing and temperature effects are active. All of these issues will be undertaken in future works.

Acknowledgments

The author thanks T Marketin for his reading of the manuscript and discussions. The support from the TÜBİTAK 2219-International Postdoctoral Research Fellowship Program is acknowledged.

References

- [1] Osterfeld F. *Rev. Mod. Phys.* **1992**, *64*, 491-557.
- [2] Harakeh, M. N.; Van Der Woude, A. *Giant Resonances. Fundamental High-Frequency Modes of Nuclear Excitation*; Clarendon Press: Oxford, UK, 2001.
- [3] Langanke, K.; Martinez-Pinedo, G. *Rev. Mod. Phys.* **2003**, *75*, 819-862.
- [4] Rapaport, J.; Taddeucci, T.; Welch, T. P.; Gaarde, C.; Larsen, J.; Horen, D. J.; Sugarbaker, E.; Koncz, P.; Foster, C. C.; Goodman, C. D. et al. *Nucl. Phys. A* **1983**, *410*, 371-398.
- [5] El-Kateb, S.; Jackson, K. P.; Alford, W. P.; Abegg, R.; Azuma, R. E.; Brown, A.; Celler, A.; Frekers, D.; Hausser, O.; Helmer, R. et al. *Phys. Rev. C* **1994**, *49*, 3128-3136.
- [6] Fracasso, S.; Colò, G. *Phys. Rev. C* **2007**, *76*, 044307.
- [7] Paar, N.; Nikšić, T.; Vretenar, D.; Ring, P. *Phys. Rev. C* **2004**, *69*, 054303.
- [8] Paar, N.; Vretenar, D.; Khan, E.; Colò, G. *Rep. Prog. Phys.* **2007**, *70*, 691-793.
- [9] Babacan, T.; Salamov, D. I.; Küçükbursa, A. *Phys. Rev. C* **2005**, *71*, 037303.
- [10] Çakmak, N.; Ünlü, S.; Selam, C. *Pramana J. Phys.* **2010**, *75*, 649-663.
- [11] Ünlü, S. *Phys. Atom. Nuclei* **2012**, *75*, 958-962.
- [12] Ünlü, S.; Çakmak, N.; Selam, C. *Nucl. Phys. A* **2017**, *957*, 491-512.
- [13] Ikeda, K.; Fujii, S.; Fujita, J. I. *Phys. Lett.* **1963**, *3*, 271-272.
- [14] Nabi, J. U.; Johnson, C. W. *J. Phys. G Nucl. Part. Phys.* **2013**, *40*, 065202.
- [15] Cole, A. L.; Anderson, T. S.; Zegers, R. G. T.; Austin, S. M.; Brown, B. A.; Valdez, L.; Gupta, S.; Hitt, G. W.; Fawwaz, O. *Phys. Rev. C* **2012**, *86*, 015809.
- [16] Caurier, E.; Langanke, K.; Martinez-Pinedo, G.; Nowacki, F. *Nucl. Phys. A* **1999**, *653*, 439-452.
- [17] Nikšić, T.; Marketin, T.; Vretenar, D.; Paar, N.; Ring P. *Phys. Rev. C* **2005**, *71*, 014308.
- [18] Paar, N.; Vretenar, D.; Marketin, T.; Ring, P. *Phys. Rev. C* **2008**, *77*, 024608.
- [19] Nabi, J. U. *Astrophys. Space Sci.* **2011**, *331*, 537-554.
- [20] Niu, Y. F.; Paar, N.; Vretenar, D.; Meng, J. *Phys. Rev. C* **2011**, *83*, 045807.
- [21] Paar, N.; Colò, G.; Khan, E.; Vretenar, D. *Phys. Rev. C* **2009**, *80*, 055801.
- [22] Fantina, A. F.; Paar, N.; Colò, G.; Khan, E.; Vretenar, D. *Phys. Rev. C* **2012**, *86*, 035805.
- [23] Dzhioev, A.; Vdovin, A. I.; Ponomarev, V. Yu.; Wambach, J.; Langanke, K.; Martínez-Pinedo, G. *Phys. Rev. C* **2010**, *81*, 015804.

- [24] Bartel, J.; Quentin, P.; Brack, M.; Guet, C.; Hakansson, H. B. *Nucl. Phys. A* **1982**, *386*, 79-100.
- [25] Niu, Y. F.; Niu, Z. M.; Colò, G.; Vigezzi, E. *Phys. Rev. Lett.* **2015**, *114*, 142501.
- [26] Bonche, P.; Levit, S.; Vautherin, D. *Nucl. Phys. A* **1984**, *427*, 278-296.
- [27] Khan, E.; Van Giai, N.; Sandulescu, N. *Nucl. Phys. A* **2007**, *789*, 94-102.
- [28] Goodman, A. L. *Nucl. Phys. A* **1981**, *352*, 30-44.
- [29] Goodman, A. L. *Nucl. Phys. A* **1981**, *352*, 45-59.
- [30] Yüksel, E.; Khan, E.; Bozkurt, K.; Colò, G. *Eur. Phys. J A* **2014**, *50*, 160-1-160-9.